

Glassy anomalies in the lattice heat capacity of a crystalline solid caused by ferroelectric fluctuationY. Ishii,^{1,*} Y. Ouchi,¹ S. Kawaguchi,² H. Ishibashi,³ Y. Kubota,³ and S. Mori¹¹*Department of Materials Science, Osaka Prefecture University, Sakai, Osaka 599-8531, Japan*²*Japan Synchrotron Radiation Research Institute (JASRI), SPring-8, Sayo, Hyogo 679-5198, Japan*³*Department of Physical Science, Osaka Prefecture University, Sakai, Osaka 599-8531, Japan*

(Received 5 February 2019; revised manuscript received 13 April 2019; published 16 August 2019)

Amorphous solids are known to exhibit excess heat capacity that shows a hump near 10 K and diverges from the Debye T^3 law at low temperature below 1 K. Here we report that these glassy features are also observed in an insulating crystalline solid. Substitutional chemical suppression of the structural phase transition temperature (T_C) of the ferroelectric oxide $\text{Ba}_{1-x}\text{Sr}_x\text{Al}_2\text{O}_4$ results in the disappearance of the T_C at $x = 0.07$. For the compositional window of $x = 0.2\text{--}0.5$, the lattice heat capacity shows a large hump below 10 K and diverges from the T^3 law below approximately 2.5 K. Synchrotron x-ray diffraction experiments on single crystals reveal the short-range correlation in the crystal structure that survives down to low temperature; this short-range correlation is responsible for the observed glasslike features in its lattice heat capacity.

DOI: [10.1103/PhysRevMaterials.3.084414](https://doi.org/10.1103/PhysRevMaterials.3.084414)**I. INTRODUCTION**

Thermal properties of structurally disordered systems have been long-standing issues for the last quarter century. Amorphous solids are generally known to exhibit low-temperature lattice heat capacity, which is quite different from that in crystals. One is a T -linear term, which is observed below 1 K in most amorphous solids [1–4] and is explained classically in terms of tunneling in two-level systems [5,6]. Another anomaly is a hump of C/T^3 around 10 K, which is generally ascribed to enhanced phonon densities of states, the so-called boson peak [7–10]. Several competing explanations have been proposed over the last few decades, which are based mainly on the following two ideas: one is localized modes distinct from acoustic modes [11–14], and another is a modification of acoustic modes due to a random fluctuation of force constants [15–17]. Recent studies have pointed out an importance of long-range correlations in amorphous solids [18] and the equivalence of the boson peak and the transverse acoustic van Hove singularity in crystal [19].

In crystals, phonons also play a key role in ferroelectric structural phase transitions. Crystals often have a phonon called a soft mode, whose frequency falls on cooling. When a soft-mode frequency eventually reaches zero, a structural phase transition occurs. Ferroelectricity is the state where macroscopic polarization arises due to inversion-symmetry breaking, which is usually caused by condensation of a soft mode and a subsequent structural phase transition. The resultant atomic displacement pattern of a ferroelectric phase reflects an associated phonon's vibration pattern. For some perovskite-type ferroelectrics called quantum paraelectrics [20–22], condensation of a soft mode is known to be suppressed down to absolute zero temperature as a result of atomic substitution or applying external pressure. In these

compounds, soft modes are known to survive even at absolute zero temperature [23]. Such a structural fluctuation was recently regarded as a kind of structural quantum critical behavior, and several predictions and evidences of superconductivity have been reported [24–26] for the widely studied quantum material SrTiO_3 .

This study highlights an improper ferroelectric, BaAl_2O_4 [27], and a Sr-substituted one [28,29] that comprise a network structure of AlO_4 tetrahedra with shared vertices. These materials crystallize in the same structure of space group $P6_322$ at high temperature over the whole compositional range. The high-temperature phase of BaAl_2O_4 possesses two acoustic soft modes with nearly the same instability [30], considered M_2 and K_2 in irreducible representation, which are characterized as collective tilting with significant vibration of oxygen atoms in the AlO_4 network. The K_2 mode is slightly unfavorable because of larger distortion in the AlO_4 tetrahedra in this mode than in the M_2 mode. As a result, the M_2 mode eventually condenses to form the corresponding low-temperature phase with a cell volume of $2a \times 2b \times c$ ($P6_3, 2a$ structure), in which the collective vibration of AlO_4 tetrahedra is frozen.

The O1 atoms, which link the AlO_4 along the c axis, vibrate with circular motion in the ab plane around the threefold axis. Because of this significant vibration, the O1 atoms exhibit anomalously large isotropic thermal factors in synchrotron x-ray structural refinements [31]. Interestingly, the T_C is strongly suppressed by a small amount of Sr substitution for Ba and disappears at $x = 0.07$ [28,29,31], as shown in Fig. 1(b). Outside the ferroelectric-paraelectric phase boundary, the isotropic thermal factor of the O1 atom exhibits an unusually large value, which is largely independent of temperature down to low temperature. This fact motivated us to investigate this compositional window in detail in expectation of observing a structurally fluctuating state lying there.

This paper reports that the $\text{Ba}_{1-x}\text{Sr}_x\text{Al}_2\text{O}_4$ crystal exhibits glasslike features in terms of its lattice heat capacity, which

*ishii@mtr.osakafu-u.ac.jp

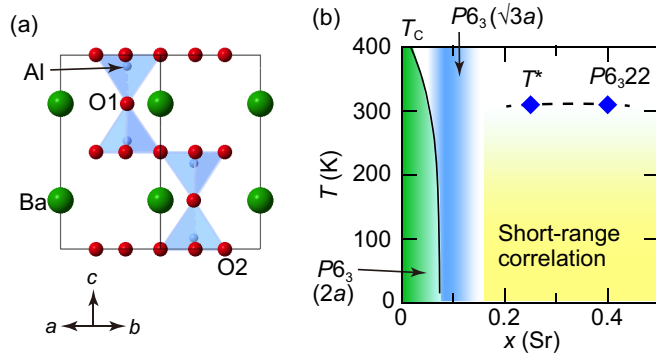


FIG. 1. (a) Crystal structure of BaAl₂O₄ of the P6₃22 phase. (b) Phase diagram of Ba_{1-x}Sr_xAl₂O₄. The T_c is rapidly suppressed by increasing x [28,29,31]. At x = 0.07, the three distinct instabilities, namely, those at the M and K points and along the Γ -A line in reciprocal space, emerge simultaneously and form superstructures. The $\sqrt{3}a$ structure, which is the ordered phase of the K₂ mode [33], exists in a narrow compositional window shaded light blue. In the region below T*, short-range correlation is dominant. The T* values are indicated by blue diamonds.

are ascribed to the short-range correlation in the atomic arrangement caused by the suppression of the structural phase transition.

II. EXPERIMENT

Single crystals of Ba_{1-x}Sr_xAl₂O₄ were grown by the self-flux method. Previously prepared Ba_{1-x}Sr_xAl₂O₄ (x = 0.2, 0.4, 0.6, 0.8) and BaCO₃ powders were mixed at a molar ratio of 6.7–8.8 to 3. Ba_{1-x}Sr_xAl₂O₄ powder was prepared by using a conventional solid-state reaction. The mixture was placed in a platinum crucible. After heating at 1650 °C for 6 h, the crucible was slowly cooled to 1440 °C–1350 °C at a rate of 2 °C/h and then cooled in a furnace to room temperature. The shiny, colorless crystals had hexagonal-shaped edges of approximately 50–100 μ m in length and were mechanically separated from the flux. The Sr concentrations of the obtained crystals were found to be x = 0.07, 0.14, 0.25, and 0.40 by means of the inductively coupled plasma method.

Synchrotron x-ray thermal diffuse scattering was performed for these single crystals over a temperature range of 100 to 400 K at the BL02B1 beamline of SPring-8. The incident x-ray radiation was set at 25 keV. The diffraction intensities were recorded on a large cylindrical image-plate camera [32]. Temperature control was performed using N₂ gas flow. Heat capacity was measured for the polycrystalline samples of x = 0–0.5 using a heat-relaxation method in a physical property measurement system (PPMS, Quantum Design). Special care was taken with regard to sample mass, thickness, and density. For the measurements, the powder sample was uniaxially pressed into a pellet and then pressed again under hydrostatic pressure. The samples were heated at 1450 °C for 48 h and cut into rectangular shapes. Typical sample thickness, mass, and density were 0.35 mm, 7 mg, and 85–90% of the theoretical values, respectively.

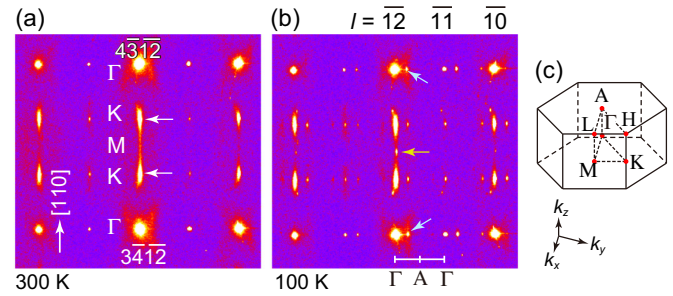


FIG. 2. Synchrotron x-ray diffraction patterns at (a) 300 K and (b) 100 K of a Ba_{1-x}Sr_xAl₂O₄ (x = 0.07) single crystal. The white arrows indicate the superlattice reflections at the K point. At 100 K, satellite reflections are visible along the Γ -A line, as marked by blue arrows. The superlattice reflection at the M point is marked by a yellow arrow. The weak reflections found just above and below the K points come from surface microcrystallites and therefore are not important. (c) The first Brillouin zone of the hexagonal crystal.

III. RESULTS AND DISCUSSION

We unexpectedly observed a curious formation of superstructures on the verge of the ferroelectric phase. Figures 2(a) and 2(b) show the synchrotron x-ray diffraction patterns of the x = 0.07 single crystal near the 4312 and 3412 fundamental reflections at 300 and 100 K, respectively. Strong superlattice reflections are observed at the K point at both temperatures, as marked by white arrows. According to Rodehorst *et al.* [33], these superlattice reflections come from the $\sqrt{3}a$ structure. In addition, weak superlattice intensity is observed at the M point at 100 K, as marked by yellow arrows, which corresponds to the 2a structure of P6₃. Furthermore, satellite reflections develop along the [001] at 100 K, as marked by blue arrows in Fig. 2(b). These satellite reflections are probably caused by the tertiary instability, which has been observed along the Γ -A line in our previous phonon calculations [30]. In other words, all of the three instabilities at K, M, and Γ -A emerge on the border of ferroelectricity.

The superlattice reflections at the K point were observed in a narrow compositional window of x = 0.07–0.14 below 400 K, which was the upper temperature limit of the present study. Notably, these reflections are significantly elongated along the [110], as shown in Figs. 2(a) and 2(b). Figure 3 shows the integrated intensity profiles plotted along [110] between two fundamental reflections obtained at 300 and 100 K for crystals of x = 0.07, 0.14, 0.25, and 0.40. $\eta = 0$ and $\eta = 1$ correspond to the reciprocal points of the lower and upper fundamental reflections, respectively. The profiles are normalized so that the fundamental reflections at $\eta = 0$ are equal in intensity.

The intensity profiles can be decomposed by using several Lorentzian functions, as shown in Fig. 3. For x = 0.07, sharp reflections are observed at the K points at 300 K. At 100 K, the superlattice intensity at the K points develops, and the additional reflection appears at the M point. As x increases, the superlattice intensity at the K point gradually decreases and the peak width becomes broader. This indicates that the long-range order of the $\sqrt{3}a$ structure is gradually suppressed and transforms to the short-range correlation. This change presumably occurs as a crossover. In addition, the peak shape

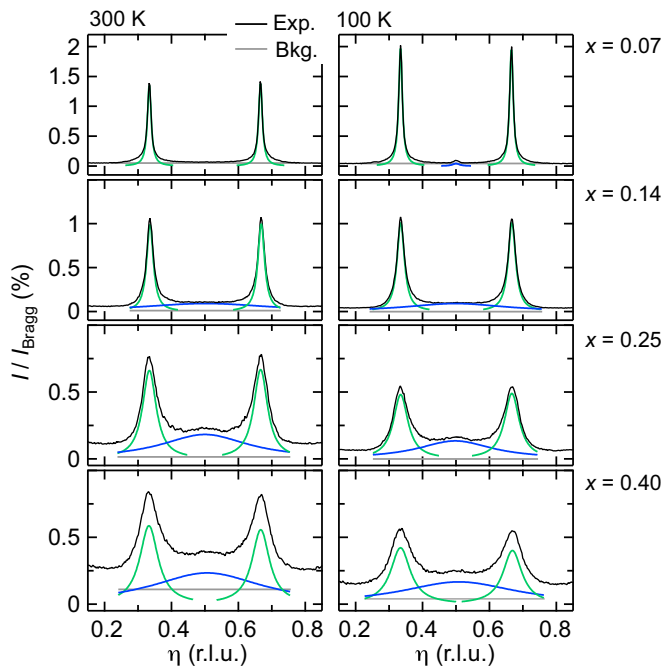


FIG. 3. Integrated intensity profiles of $x = 0.07$ – 0.40 plotted along the $[110]$ direction at 300 K (left) and 100 K (right). $\eta = 0$ and 1 correspond to reciprocal points of the lower and upper fundamental reflections, respectively. They are fitted using several Lorentzian functions shown by green and blue lines. Gray lines show backgrounds. Fitting results for other temperatures are shown in the Supplemental Material [34].

of each profile at the K point becomes asymmetric for $x \geq 0.14$. This indicates the existence of a broad peak at the center of the two K-point peaks, at the M point, as shown by blue lines.

The maximum intensity of the peak (I_p/I_{Bragg}) at the K points and the full width at half maximum (FWHM) are plotted against temperature in Figs. 4(a) and 4(b), respectively. The temperature dependence differs among these samples. The intensity shows sharp enhancement for $x = 0.07$ below 200 K but becomes nearly flat for $x = 0.14$. For $x \geq 0.25$, each intensity takes a maximum near 300 K, as denoted by T^* , and decreases below T^* . As shown in Fig. 4(b), the FWHM of $x = 0.07$ slightly decreases as a consequence of development of the superlattice intensity below 200 K. The FWHM of other compositions systematically increases as temperature decreases. Although qualitative discussion about the broad feature at the M point is difficult due to the very weak intensity, the temperature dependence of the intensity and FWHM of these broad peaks are shown in the Supplemental Material [34].

We have also performed electron diffraction experiments on the crushed single crystal of $x = 0.14$. In contrast to the x-ray diffraction experiments described above, the scattering at the K point was diffusive and disappeared at 155 K upon cooling, below which only the diffuse scatterings at the M point were observed instead of the superlattice reflections at the K points. Similar results have also been observed in our previous electron diffraction experiments using powder samples [28]. These facts mean the superlattice reflections at

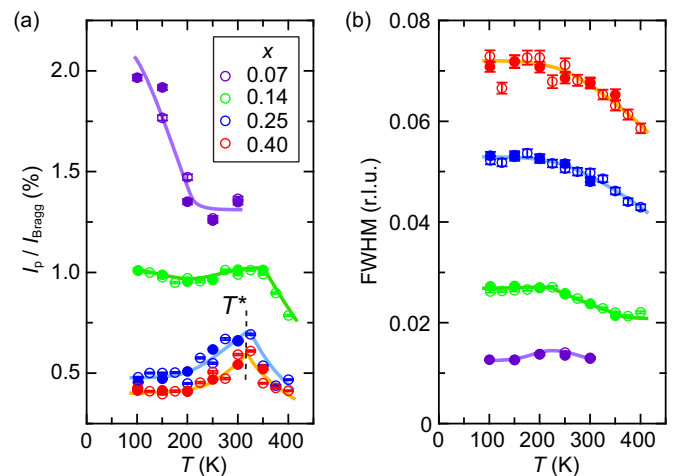


FIG. 4. (a) Normalized peak intensity (I_p/I_{Bragg}) and (b) FWHM at the K points plotted against temperature. For $x \geq 0.25$, each plot shows a maximum at approximately 300 K, as denoted by T^* . The open and solid symbols represent the data obtained upon heating and cooling, respectively. Solid lines are guides for the eye.

the K point are strongly affected by extrinsic factors such as strain energy due to small grain size. Further information is described in Fig. S5 in the Supplemental Material [34].

Although Sr substitution would slightly affect the phonon dispersion, it would not substantially change the essential character of the soft modes. The enhancement in the peak intensity at T^* observed in Fig. 4(a) is simply attributable to the reduction in the phonon frequencies, ω , because the thermal diffuse scattering intensity caused by phonon scales as ω^{-2} . That is, the K_2 mode reduces the phonon frequency towards T^* , although it cannot condense completely. There are two possible pictures for the weakly correlated disorder below the T^* : the first is the soft modes that survive in this state as dynamic disorder, and the second is the glasslike short-range correlation as static disorder caused by the incomplete condensation of the soft modes.

Figure 5(a) shows the heat capacity divided by T^3 plotted against T on a logarithmic scale. Figure 5(b) shows the enlarged view of $T \leq 8$ K plotted on a linear scale. Polycrystalline samples of $x = 0$ – 0.5 were used for the measurements. The C/T^3 of $x = 0$ follows the Debye T^3 law and shows a constant value below 4 K. The Debye temperature (Θ_D) is evaluated to be 428 K from the coefficient. The $x = 1$ crystal, the end material of the Sr-rich side, also follows this T^3 law. However, for $x = 0.2$ – 0.5 crystals, the heat capacity surprisingly diverges from this T^3 law below approximately 2.5 K, as shown in Fig. 5. In addition, a large enhancement in C/T^3 is observed for $x \geq 0.07$ below 10 K.

These two features are very similar to those observed in amorphous solids, such as amorphous SiO_2 . That is, the lattice heat capacity of amorphous solids varies as $c_1 T + c_2 T^3$ below 1 K and shows a hump of C/T^3 at approximately 10 K [1–4]. Although the mechanism is still under debate [9–13,15,16], the excess heat capacity observed in the amorphous system has generally been accepted to arise from the enhanced density of states [7–10] of acoustic phonons caused by the disordered structure [17,19]. Obviously, the glassy upturn

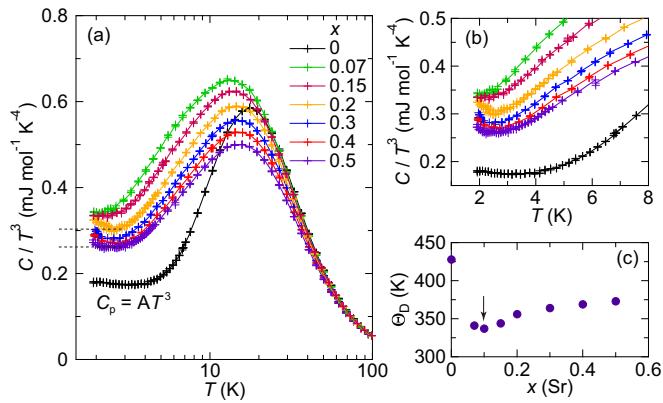


FIG. 5. (a) The lattice heat capacity (C_p) divided by T^3 is plotted against temperature. Enhanced lattice heat capacity near 10 K is observed for $x \geq 0.07$. In addition, the $x = 0.2$ – 0.5 samples show an upturn below ≈ 2.5 K, which is typical behavior in amorphous solids. (b) Enlarged view of $T \leq 8$ K plotted on a linear scale. (c) Debye temperature (Θ_D) obtained by using the coefficient of C/T^3 . For $x = 0.2$ – 0.5 , the coefficient of C/T^3 was determined by using the local minimum value, as indicated by broken lines in (a).

observed in the present system is attributable to the disordered state found below T^* .

Figure 5(c) shows the Debye temperature (Θ_D) plotted against x . These values were obtained from the coefficients of C/T^3 for $x = 0$ – 0.15 . For $x \geq 0.2$, the local minimum values of C/T^3 were used for the calculation, as shown by broken lines in Fig. 5(a). Θ_D exhibits a valley near $x = 0.1$, indicating that the Debye frequency rapidly decreases towards the ferroelectric-paraelectric phase boundary. A similar decrease in Θ_D has been reported near a quantum critical point of $(\text{Ca}_x\text{Sr}_{1-x})_3\text{Rh}_4\text{Sn}_{13}$, in which interplay of superconductivity and structural quantum fluctuation has been discussed [35].

The above results can be summarized as follows. The $\sqrt{3}a$ structure exists in a narrow compositional window right next to the ferroelectric $2a$ structure. This $\sqrt{3}a$ structure is the condensed state of the K_2 mode [33]. Because the condensation of the M_2 mode is suppressed outside the ferroelectric-paraelectric phase boundary, the secondary instability at the K point temporarily appears. Simultaneously, the tertiary instability along Γ -A also emerges. However, the condensed state of the K_2 mode is inherently unfavorable in terms of Coulomb energy. In addition, the instability at Γ -A is very small [30].

For these reasons, these temporarily emerged states are easily destroyed by a further increase in x . In the fluctuation state below T^* , the lattice heat capacity exhibits glassy behavior. A further increase in x turns into the $P2_1$ phase in the Sr-rich side [36], which is another condensed form of the M_2 mode [37].

One may expect that the substitution of Sr having a smaller ionic size would make the structural phase transition more likely to occur, because the cell volume contracts with the Sr concentration. However, the structural phase transition is actually suppressed by the Sr substitution. According to our structural refinements, in fact, the average position of Ba and Sr atoms tends to shift along the c direction from the original $2b$ site of the $P6_322$ crystal structure [31]. The magnitude of this displacement increases with the Sr concentration, which means the displacement absorbs strains caused by the volume contraction and AlO_4 tilting. This would lower the local symmetry at each constituent atom. Local structural analyses, such as pair distribution function analysis, will explain the situation more clearly.

IV. CONCLUSION

We have discovered glasslike features at low temperature in terms of the lattice heat capacity of $\text{Ba}_{1-x}\text{Sr}_x\text{Al}_2\text{O}_4$, which is in a structurally disordered state outside the ferroelectric phase. In this state, the structural fluctuation associated with short-range correlation is dominant as a consequence of the suppression of the M_2 and K_2 modes. This short-range correlation is responsible for the glasslike features observed in the low-temperature lattice heat capacity.

ACKNOWLEDGMENTS

We thank Prof. T. Doi (Kyoto University) and Prof. S. Horii (Kyoto University of Advanced Science) for their support in the compositional analysis using the inductively coupled plasma method. We also thank Dr. K. Sugimoto (JASRI) for his kind help in single crystal x-ray diffraction experiment. This work was supported by a JSPS Grant-in-Aid for Scientific Research on Innovative Areas “Mixed-anion” (Grant No. 17H05487) and JSPS KAKENHI (Grant No. 17K14323). The synchrotron radiation experiments were performed at BL02B1 of SPring-8 with the approval of the Japan Synchrotron Radiation Research Institute (JASRI) (Proposal No. 2017B1460).

- [1] R. C. Zeller and R. O. Pohl, *Phys. Rev. B* **4**, 2029 (1971).
- [2] L. Gil, M. A. Ramos, A. Bringer, and U. Buchenau, *Phys. Rev. Lett.* **70**, 182 (1993).
- [3] M. Mertig, G. Pompe, and E. Hegenbarth, *Solid State Commun.* **49**, 369 (1984).
- [4] D. R. Queen, X. Liu, J. Karel, T. H. Metcalf, and F. Hellman, *Phys. Rev. Lett.* **110**, 135901 (2013).
- [5] W. A. Phillips, *J. Low Temp. Phys.* **7**, 351 (1972).
- [6] P. W. Anderson, B. I. Halperin, and C. M. Varma, *Philos. Mag.* (1798-1977) **25**, 1 (1972).
- [7] U. Buchenau, N. Nücker, and A. J. Dianoux, *Phys. Rev. Lett.* **53**, 2316 (1984).
- [8] U. Buchenau, M. Prager, N. Nücker, A. J. Dianoux, N. Ahmad, and W. A. Phillips, *Phys. Rev. B* **34**, 5665 (1986).
- [9] V. Malinovsky and A. Sokolov, *Solid State Commun.* **57**, 757 (1986).
- [10] T. Nakayama, *Rep. Prog. Phys.* **65**, 1195 (2002).
- [11] B. B. Laird and H. R. Schober, *Phys. Rev. Lett.* **66**, 636 (1991).
- [12] E. Duval, A. Boukenter, and T. Achibat, *J. Phys.: Condens. Matter* **2**, 10227 (1990).
- [13] H. Tanaka, *J. Phys. Soc. Jpn.* **70**, 1178 (2001).
- [14] U. Buchenau, Yu. M. Galperin, V. L. Gurevich, and H. R. Schober, *Phys. Rev. B* **43**, 5039 (1991).

- [15] W. Schirmacher, G. Diezemann, and C. Ganter, *Phys. Rev. Lett.* **81**, 136 (1998).
- [16] S. N. Taraskin, Y. L. Loh, G. Natarajan, and S. R. Elliott, *Phys. Rev. Lett.* **86**, 1255 (2001).
- [17] H. Shintani and H. Tanaka, *Nat. Mater.* **7**, 870 (2008).
- [18] S. Gelin, H. Tanaka, and A. Lematre, *Nat. Mater.* **15**, 1177 (2016).
- [19] A. I. Chumakov, G. Monaco, A. Monaco, W. A. Crichton, A. Bosak, R. Rüffer, A. Meyer, F. Kargl, L. Comez, D. Fioretto, H. Giefers, S. Roitsch, G. Wortmann, M. H. Manghnani, A. Hushur, Q. Williams, J. Balogh, K. Parliński, P. Jochym, and P. Piekarczyk, *Phys. Rev. Lett.* **106**, 225501 (2011).
- [20] K. A. Müller and H. Burkard, *Phys. Rev. B* **19**, 3593 (1979).
- [21] G. A. Samara and B. Morosin, *Phys. Rev. B* **8**, 1256 (1973).
- [22] H. Taniguchi, H. P. Soon, T. Shimizu, H. Moriwake, Y. J. Shan, and M. Itoh, *Phys. Rev. B* **84**, 174106 (2011).
- [23] H. Taniguchi, M. Itoh, and T. Yagi, *Phys. Rev. Lett.* **99**, 017602 (2007).
- [24] S. E. Rowley, L. J. Spalek, R. P. Smith, M. P. M. Dean, M. Itoh, J. F. Scott, G. G. Lonzarich, and S. S. Saxena, *Nat. Phys.* **10**, 367 (2014).
- [25] J. M. Edge, Y. Kedem, U. Aschauer, N. A. Spaldin, and A. V. Balatsky, *Phys. Rev. Lett.* **115**, 247002 (2015).
- [26] C. W. Rischau, X. Lin, C. P. Grams, D. Finck, S. Harms, J. Engelmayer, T. Lorenz, Y. Gallais, B. Fauqué, J. Hemberger, and K. Behnia, *Nat. Phys.* **13**, 643 (2017).
- [27] H. T. Stokes, C. Sadate, D. M. Hatch, L. L. Boyer, and M. J. Mehl, *Phys. Rev. B* **65**, 064105 (2002).
- [28] Y. Ishii, H. Tsukasaki, E. Tanaka, and S. Mori, *Sci. Rep.* **6**, 19154 (2016).
- [29] Y. Ishii, H. Tsukasaki, E. Tanaka, S. Kawaguchi, and S. Mori, *Phys. Rev. B* **94**, 184106 (2016).
- [30] Y. Ishii, S. Mori, Y. Nakahira, C. Moriyoshi, J. Park, B. G. Kim, H. Moriwake, H. Taniguchi, and Y. Kuroiwa, *Phys. Rev. B* **93**, 134108 (2016).
- [31] S. Kawaguchi, Y. Ishii, E. Tanaka, H. Tsukasaki, Y. Kubota, and S. Mori, *Phys. Rev. B* **94**, 054117 (2016).
- [32] K. Sugimoto, H. Ohsumi, S. Aoyagi, E. Nishibori, C. Moriyoshi, Y. Kuroiwa, H. Sawa, and M. Takata, in *10th International Conference on Radiation Instrumentation SRI 2009*, edited by R. Garrett, I. Gentle, K. Nugent, and S. Wilkins, AIP Conf. Proc. No. 1234 (AIP, New York, 2010), p. 887.
- [33] U. Rodehorst, M. Carpenter, S. Marion, and C. Henderson, *Mineral. Mag.* **67**, 989 (2003).
- [34] See Supplemental Material at <http://link.aps.org/supplemental/10.1103/PhysRevMaterials.3.084414> for (i) detailed information for the experimental procedure, (ii) fitting results for the diffuse scattering profiles, and (iii) several electron diffraction patterns of the $x = 0.14$ single crystals used for the x-ray diffraction experiments.
- [35] W. C. Yu, Y. W. Cheung, P. J. Saines, M. Imai, T. Matsumoto, C. Michioka, K. Yoshimura, and S. K. Goh, *Phys. Rev. Lett.* **115**, 207003 (2015).
- [36] Y. Ishii, H. Tsukasaki, S. Kawaguchi, Y. Ouchi, and S. Mori, *J. Solid State Chem.* **249**, 149 (2017).
- [37] J. M. Perez-Mato, R. L. Withers, A.-K. Larsson, D. Orobengoa, and Y. Liu, *Phys. Rev. B* **79**, 064111 (2009).